PAPER • OPEN ACCESS

Quantum dynamics of trapped ions in a dynamic field gradient using dressed states

To cite this article: Sabine Wölk and Christof Wunderlich 2017 *New J. Phys.* **19** 083021

New Journal of Physics
The open access journal at the forefront of physics

Deutsche Physikalische Gesellschaft DPG
IOP Institute of Physics

Published in partnership with: Deutsche Physikalische Gesellschaft and the Institute of Physics

OPEN ACCESS

RECEIVED
13 September 2016

REVISED
5 June 2017

ACCEPTED FOR PUBLICATION
22 June 2017

PUBLISHED
21 August 2017

PAPER

Quantum dynamics of trapped ions in a dynamic field gradient using dressed states

Sabine Wölk[1] **and Christof Wunderlich**

Department Physik, Naturwissenschaftlich-Technische Fakultät, Universität Siegen, D-57068 Siegen, Germany
[1] Author to whom any correspondence should be addressed.

E-mail: woelk@physik.uni-siegen.de

Keywords: trapped ions, radio frequency radiation, spin–spin coupling, addressing, dressed states

Abstract

Novel ion traps that provide either a static or a dynamic magnetic gradient field allow for the use of radio-frequency radiation for coupling internal and motional states of ions, which is essential for conditional quantum logic. We show that the Hamiltonian describing this coupling in the presence of a resonant dynamic gradient, is identical, in a dressed state basis, to the Hamiltonian in the case of a static gradient. The coupling strength is in both cases described by the same effective Lamb-Dicke parameter. This insight can be used to overcome demanding experimental requirements when using a dynamic gradient field for state-of-the-art experiments with trapped ions, for example, in quantum information science. At the same time, this insight opens new experimental perspectives by way of using a single resonant or detuned dynamic gradient field, inducing long-range coupling, for conditional multi-qubit dynamics.

1. Introduction

Experiments with atomic trapped ions have played a leading role in the development of experimental quantum information science [1–3]. Well isolated from their environment, trapped ions are ideally suited for investigating fundamental questions of quantum physics, and are a promising candidate for quantum simulations and scalable universal quantum computing reaching beyond the capabilities of classical computers [4]. Internal electronic states serving as qubits are coherently prepared using electromagnetic radiation in the optical or radio-frequency (RF) regime, and an upper limit for the coherence time of ionic qubits is set by the coherence time of this radiation. For conditional quantum dynamics with two or more qubits, represented by several ions confined in the same trap or trapping region, the collective vibrational motion is coupled to the internal dynamics of individual ions, thus serving as a quantum bus.

Using laser light for coupling ionic qubits via this quantum bus has been standard for some decades, since only with light in and around the visible regime the Lamb-Dicke parameter η, measuring the coupling strength between internal and motional states [5], takes on a sufficiently large value in typical traps. Driving solely a single desired ion out of a collection of trapped ions, typically spaced apart by a few micrometers, also required optical radiation that can be focused down to a spot size smaller than the inter-ion separation. In numerous experiments laser light has been successfully used to deterministically prepare quantum states of trapped ions, even complete quantum algorithms [6, 7] and quantum simulations [8, 9] have been implemented.

The complexity of experimental set-ups can be reduced decisively, when RF radiation is used to directly drive the ions' dynamics instead of taking the detour of imprinting RF signals onto optical beams and then steering these optical beams towards trapped ions. With laser beams, frequency-, phase-, and amplitude noise, diffraction and beam pointing instabilities in the optical domain pose additional problems that can be avoided by the direct use of RF radiation.

Using RF radiation for coupling internal and motional dynamics becomes possible when an additional, spatially varying field is applied to an atom trap. This can be a static [10] or a dynamic [11] magnetic gradient field. In both cases, an effective Lamb-Dicke parameter arises through magnetic gradient induced coupling (MAGIC) even upon excitation with RF radiation [12–17]. In addition, individual addressing of atoms using RF radiation has been shown to be effective [12, 14, 16, 18–21].

When employing MAGIC for trapped ions as a complementary approach to successful research based on laser-driven ion trap quantum logic, spontaneous emission because of the finite lifetime of qubit states, or spontaneous scattering caused by non-resonant laser light driving Raman transitions is not a concern for the coherence time of qubits. As is the case for some laser-based gates [22], conditional quantum dynamics based on magnetic gradient induced spin–spin coupling is tolerant against thermal excitation of the ions' vibrational motion.

Single-qubit quantum gates driven by RF radiation have been implemented with an error well below 10^{-4} [23, 24], an important threshold for fault-tolerant quantum computing. Using a static field gradient, a quantum byte (eight ions) could be addressed with a measured cross-talk between closely spaced, interacting ions in the 10^{-5} range [20]. MAGIC was also employed to demonstrate two-qubit gates [13, 14, 17, 25], three-qubit gates [26], and opens new possibilities for quantum simulations and quantum computation [26, 27].

In this paper we show that the addition of either a static or a dynamic gradient field to a Coulomb crystal of trapped ions—in order to take advantage of MAGIC—can be described by similar Hamiltonians. It is shown that the Hamiltonian in a dressed-state picture, obtained when applying a spatially varying resonant dynamic field, is identical to the case of having a static gradient field and a spatially constant qubit driving field.

In current experiments where a dynamic gradient field is applied, great care is taken to null the dynamic magnetic field at the ions' positions and thus to retain only a gradient of the dynamic field at this position [13, 28, 29] in order to obtain high-fidelity two-qubit gates. Another approach is to use an extra dressing field to reduce errors resulting from a non-zero offset field [25]. Here, we show how atomic states dressed by the dynamic magnetic gradient field itself could be employed for conditional quantum gates, thus decisively simplifying experimental efforts necessary when implementing the dynamic MAGIC scheme.

Before introducing the novel scheme and discussing it in more detail, we briefly summarize its features: (i) It dispenses with the demanding need to null the dynamic field at the ions' locations. This could be particularly important when implementing conditional quantum dynamics with more than two ions. (ii) Atomic states dressed by the dynamic gradient field are insensitive to ambient field noise making it superfluous to apply a relatively strong and stable bias field in order to create qubits with long coherence time (so-called clock states). (iii) Applying a dynamic gradient field with the gradient pointing along the axis of weakest confinement of ions in a linear trap becomes feasible, and, thus can decidedly enhance the coupling strength between qubit states and motional states. (iv) It becomes straightforward to individually address ions exposed to such a dynamic field gradient with low cross-talk. (v) It is shown that long-range spin–spin coupling between dressed qubits arises when applying a *single* dynamic gradient field. Conditional dynamics arising from this coupling could be used for quantum simulations and efficient quantum computation.

In what follows, we consider coupling between internal and motional states in the presence of a static (section 2) or a dynamic (section 3) magnetic gradient field. We recapitulate both methods and bring them into a common representation starting by first considering a single atom before demonstrating their similarity for multi-qubit systems.

2. Static magnetic gradient

In this section we first outline how the application of a static magnetic field gradient to a single trapped atom gives rise to coupling between the atom's internal and motional states. The summary below is based on results published in [10] and illustrated, for instance, in [30]. Then, a collection of ions exposed to a magnetic gradient field is considered, and the expression describing the coupling between internal states of different ions (spin–spin coupling) induced by the gradient field is given. The derivation of this expression for spin–spin coupling can be found in [31] (see also [12, 32] for physical interpretations). We include this material here to make the present article reasonably self-contained and to establish the notation.

For a static magnetic gradient parallel to the z-axis, the Hamiltonian describing a single atom j with energy level spacing $\hbar\omega_0$ confined in a harmonic trap at position z_j expanded up to first order in the field gradient is given by

$$H_{\text{static}} = \frac{1}{2}\hbar\omega_0\sigma_z^{(j)} + \frac{\mu_z}{2}(B_0 + zB')\sigma_z^{(j)} + \hbar\nu_n a_n^\dagger a_n, \tag{1}$$

with the ion's matrix element of the magnetic dipole moment μ_z, the magnetic field $B(z) = B_0 + zB'$, and the Pauli-z matrix σ_z. Here, $a_n^\dagger$ and a_n describe the creation and annihilation operators of the vibrational mode in the harmonic trap with angular frequency ν_n. The position z of ion j is given by $z = z_j + \Delta z_j$ with its equilibrium position z_j and the displacement Δz_j. The displacement can be written in terms of the normal vibrational mode n as

$$\Delta z_j = b_{j,n} q_n (a_n + a_n^\dagger) \tag{2}$$

with the help of the coefficients $-1 \leqslant b_{j,n} \leqslant 1$ that reflect how strongly ion j participates in motional mode n (if only a single ion is considered, then $b_{1,1} \equiv 1$). Here, $q_n = \sqrt{\hbar/(2m\nu_n)}$ describes the atom's spatial extent in the ground state of the harmonic trapping potential. As a consequence, Hamiltonian equation (1) can be rewritten as

$$H_{\text{static}} = \frac{1}{2}\hbar\omega(z_j)\sigma_z^{(j)} + \hbar\nu_n a_n^\dagger a_n + \hbar\nu_n \varepsilon_{j,n}(a_n^\dagger + a_n)\sigma_z^{(j)} \tag{3}$$

with the position dependent level splitting $\omega(z_j) = \omega_0 + \mu_z(B_0 + z_j B')/\hbar$ and the coupling strength[2]

$$\varepsilon_{j,n} = \frac{(\mu_z B' b_{j,n} q_n)}{(2\hbar\nu_n)}. \tag{4}$$

In this way, an interaction between the internal and external degrees of freedom is created whenever a qubit with position dependent level splitting is used. No additional lasers or RF radiation are needed to create this interaction. Note that B' indicates the magnitude of the static magnetic field gradient.

Now, we consider the application of an additional driving field with angular frequency ω_D close to the atomic resonance $\omega(z_j)$. The interaction between this driving field and the trapped atom is described by

$$H_D = \frac{\hbar\Omega_D}{2}\sigma_x^{(j)}\exp[\mathrm{i}(kz - \omega_D t)] + \text{h.c.} \tag{5}$$

with k being the projection of the wave vector $\vec{k}$ of the driving field onto the z-direction. An expansion of z around its equilibrium position reveals an interaction between internal and external degrees of freedom whose strength is governed by the Lamb-Dicke parameter $\eta = b_{j,n} q_n k$ [5]. However, when the applied radiation has a long wavelength λ, for instance in the RF regime, then the wavenumber $k = 2\pi/\lambda$ is too small (in typical ion traps) to yield a sizable η, and, thus the coupling between internal and motional states, that would make excitation of motional sidebands effective, is negligible. A small value of k can be interpreted as the linear momentum $\hbar k$ transferred to the atom upon absorption or emission of a photon being too small to change the trapped atom's motional state. However, in the presence of a gradient field (equations (1), (3) and (4)) motional sideband excitation by a driving field (equation (5)) becomes effective as outlined below.

The transformation $\tilde{H} = \mathrm{e}^{S_{j,n}} H \mathrm{e}^{-S_{j,n}}$ [10] of H_{static} (equation (1)) leads to decoupling of internal and external degrees of freedom and we obtain

$$\tilde{H}_{\text{static}} = \frac{\hbar\omega_j}{2}\sigma_z^{(j)} + \hbar\nu_n \tilde{a}_n^\dagger \tilde{a}_n. \tag{6}$$

The operator $S_{j,n}$ for a single ion j and mode n is given by

$$S_{j,n} = \varepsilon_{j,n}(a_n^\dagger - a_n)\sigma_z^{(j)}, \tag{7}$$

signifying an internal-state dependent shift of the normal modes induced by the magnetic gradient.

The same transformation applied to the driving field Hamiltonian (equation (5)), $\tilde{H}_D = \mathrm{e}^{S_{j,n}} H_D \mathrm{e}^{-S_{j,n}}$ yields [10]

$$\tilde{H}_D = \frac{\hbar\Omega_D}{2}(\sigma_+ \mathrm{e}^{\varepsilon_{j,n}(\tilde{a}_n^\dagger - \tilde{a}_n)} + \sigma_- \mathrm{e}^{-\varepsilon_{j,n}(\tilde{a}_n^\dagger - \tilde{a}_n)})(\mathrm{e}^{\mathrm{i}\omega_D t} + \mathrm{e}^{-\mathrm{i}\omega_D t}), \tag{8}$$

which reveals the role of $\varepsilon_{j,n}$ as a generalized Lamb-Dicke parameter. Expanding $\tilde{H}_D$ in $\varepsilon_{j,n}$ shows that motional sidebands of the internal resonance can be resonantly driven, for instance, if $\omega_D = \omega_j \pm \nu_n$.

In the summary above we already established the notation for N ions ($1 \leqslant j,\ n \leqslant N$) even though, so far, a single harmonically trapped atom ($j \equiv 1,\ n \equiv 1$) was considered. Now, we turn to the case of N ions confined in a linear trap: the generalization of equation (3) to N ions and its transformation by $\mathrm{e}^S H_{\text{static}} \mathrm{e}^{-S}$ with $S = \sum_{j,n} S_{j,n}$ leads to [31]

$$\tilde{H}_{\text{static}} = \frac{1}{2}\sum_j \hbar\omega(z_j)\sigma_z^{(j)} + \sum_n \hbar\nu_n \tilde{a}_n^\dagger \tilde{a}_n - \frac{\hbar}{2}\sum_{j<k} J_{j,k}\sigma_z^{(j)}\sigma_z^{(k)}. \tag{9}$$

This reveals a direct interaction of the internal degrees of freedom: a long-range interaction between the ions' internal states (henceforth referred to as spins) induced by the static magnetic gradient described by

$$H_J = -\frac{\hbar}{2}\sum_{j<k} J_{j,k}\sigma_z^{(j)}\sigma_z^{(k)}, \tag{10}$$

[2] Equation (4) is valid in the regime of a linear Zeeman effect. In more general cases the coupling strength is given by $\varepsilon_{j,n} = |\partial_z \omega_j| b_{j,n} q_n/\nu_n$ where ω_j can be determined e.g. by the Breit–Rabi formula.

with the coupling strength given by [31, 32, 43]

$$J_{j,k} = \sum_n \nu_n \varepsilon_{j,n} \varepsilon_{k,n}. \tag{11}$$

Again, we note that this interaction is induced solely by the magnetic gradient without any additional radiation. Furthermore, this spin–spin coupling is independent of the motional degrees of freedom and enables therefore so called hot quantum gates, as long as the total potential confining the ions (the external trapping potential plus the Coulomb interaction between the ions) remains a harmonic potential.

3. Dynamic magnetic gradient

The scheme described by Ospelkaus *et al* [11] allows for spin–spin coupling via a dynamic magnetic field $B(z, t) = \cos(\omega_B t) B(z)$, with a gradient of the amplitude perpendicular to the string of ions. When recapitulating this scheme in what follows, we take the gradient of this dynamic magnetic field to point along the z-axis. Thus, the string of ions is taken to be parallel to the x-axis and parallel to the electrode providing the oscillating magnetic fields and the ion and the magnetic field are coupled via the matrix element μ_x of the magnetic dipole moment[3]. In analogy to the static case, we express the position z via the equilibrium position z_j plus a small displacement Δz and expand the magnetic field $B(z) = B_j + \Delta z B'$ around z_j. In this way, we arrive at the Hamiltonian of a single ion j coupled to the radial mode n

$$\begin{aligned} H_{\text{osci}} = \frac{\hbar\omega_0}{2}\sigma_z^{(j)} + \hbar\nu_n a_n^\dagger a_n + \sigma_x^{(j)} \cos(\omega_B t)\mu_x B_j \\ + \sigma_x^{(j)} \cos(\omega_B t)\mu_x B' [b_{j,n} q_n (a_n^\dagger + a_n)]. \end{aligned} \tag{12}$$

As a consequence, the interaction Hamiltonian in the rotating wave approximation (RWA) is given by

$$H_{\text{osci,I}} = \hbar\sigma_+ (\Omega_j e^{-i\delta t} + \Omega_{j,n} a_n e^{-i(\delta+\nu_n)t}) + \text{h.c.} \tag{13}$$

with the detuning $\delta = \omega_B - \omega_0$, the Rabi frequencies

$$\Omega_j = B_j \mu_x / (2\hbar), \tag{14}$$

and

$$\Omega_{j,n} = B' \mu_x b_{j,n} q_n / (2\hbar). \tag{15}$$

Similar to the static case, the coupling between internal and motional degrees of freedom is caused by the magnetic gradient (equations (12) and (13)).

By applying two dynamic magnetic fields with equal amplitude and opposite detuning close to the red- and blue sideband, a spin–spin interaction can be generated [11]. In general, a spin–spin interaction without additional excitations via the carrier transition is desirable. Excitation via the carrier is suppressed due to off-resonant excitation (detuning of the driving fields by about ν_n), and it can be neglected if $\Omega_j \ll \nu_n$. This leads, together with equation (14), to the restriction $\mu_x B_j \ll \hbar\nu_n$ for the magnetic field. Typical magnitudes are $\nu_n = 2\pi \times 10^6$ Hz and $\hbar/\mu_B = 10^{-10}$ T Hz^{-1}, which leads to $B_j \ll 10^{-4}$ T. As a consequence, a high magnetic gradient and a small absolute magnetic field strength are needed for high-fidelity two-qubit gates. Therefore, considerable experimental effort is devoted to an exact geometry of the electrodes generating the magnetic fields and to exact positioning of the ions [13, 28, 29].

4. Dynamic MAGIC in a dressed-state basis

In what follows, we show that the approach using a resonant dynamic magnetic gradient for coupling internal and external degrees of freedom is equivalent to the static gradient approach when expressing the Hamiltonian for the dynamic case in a dressed-states basis. Furthermore, it is outlined how a non-resonant dynamic gradient allows for interesting variations of spin-motion coupling.

For this purpose, we transform the Hamiltonian H_{osci} given in equation (12) into the rotating frame of the ion with $\delta = \omega_B - \omega_0$, resulting in

$$H_I = \frac{\mu_x}{2}(\sigma_+ e^{-i\delta t} + \sigma_- e^{i\delta t}) \times [B_j + B' b_{j,n} q_n (a_n^\dagger + a_n)] + \hbar\nu_n a_n^\dagger a_n \tag{16}$$

for a single ion and a single mode.

[3] For details on the matrix elements μ_z and μ_x see [11].

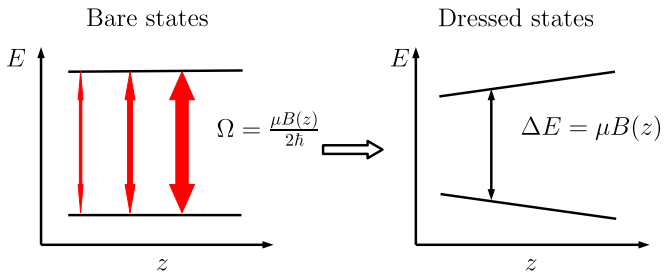

Figure 1. Left: the interaction strength Ω between a spatially varying driving field $B(z, t) = B(z)\cos(\omega_B t)$ and a two-level atom. Right: in the dressed-state picture this position dependent interaction leads to a position dependent level splitting ΔE of states $|\pm\rangle$.

The eigenstates of the operator $\sigma_+ \exp(-\mathrm{i}\delta t) + \sigma_- \exp(\mathrm{i}\delta t)$ are given by

$$|\pm\rangle = \frac{1}{\sqrt{2}}(\mathrm{e}^{\mathrm{i}\delta t/2}|g\rangle \pm \mathrm{e}^{-\mathrm{i}\delta t/2}|e\rangle) \tag{17}$$

with the bare atomic states $|g\rangle$ and $|e\rangle$. The states $|\pm\rangle$ are equivalent to the often used time-independent dressed states for $\delta = 0$. For $\delta \neq 0$ the states $|\pm\rangle$ deviate from the dressed states and become time dependent (for a detailed comparison with the usual dressed states for $\delta \neq 0$ see section 4.1). As a consequence, the Pauli-z matrix in the basis $|\pm\rangle$ is given by

$$\Sigma_z = T(\sigma_+\mathrm{e}^{-\mathrm{i}\delta t} + \sigma_-\mathrm{e}^{\mathrm{i}\delta t})T^\dagger \tag{18}$$

with the unitary transformation

$$T = \frac{\mathrm{e}^{-\mathrm{i}\delta t/2}}{\sqrt{2}}\Big(|+\rangle + |-\rangle\Big)\langle g| + \frac{\mathrm{e}^{\mathrm{i}\delta t/2}}{\sqrt{2}}\Big(|+\rangle - |-\rangle\Big)\langle e|. \tag{19}$$

This relation shows that the strength of the interaction between the bare states (proportional to $\sigma_+ + \sigma_-$) transforms into the level splitting of the states $|\pm\rangle$ (proportional to Σ_z) as displayed in figure 1.

The Hamiltonian $\hbar\nu_n a_n^\dagger a_n$ describing the energy of the vibrational modes is invariant under all these transformations. As a consequence, the resulting Hamiltonian $H_{|\pm\rangle} = THT^\dagger + \mathrm{i}(\mathrm{d}_t T(t))T^\dagger(t)$ leads to

$$H_{|\pm\rangle} = \frac{\mu_x B_j}{2}\Sigma_z + \hbar\nu_n a_n^\dagger a_n + \frac{\mu_x B' b_{j,n} q_n}{2}(a_n^\dagger + a_n)\Sigma_z + \frac{\hbar\delta}{2}\Sigma_x. \tag{20}$$

The first three terms exhibit exactly the same form as the Hamiltonian of the static gradient field given in equation (3). The last term results from the fact that for $\delta \neq 0$ the transformation matrix T becomes time dependent, leading to an additional term. A comparison of the Hamiltonians $H_\pm$, equation (20), and H_{static}, equation (3), leads to the identifications

$$\omega(z_j) = \frac{\mu_x B_j}{\hbar} \tag{21}$$

and

$$\varepsilon_{j,n} = \frac{\mu_x B' b_{j,n} q_n}{2\hbar\nu_n}. \tag{22}$$

A comparison with equation (4) reveals that the coupling between motional and internal degrees of freedom in static and dynamic MAGIC are not only of the same form but are described by exactly the same effective Lamb-Dicke parameter using the appropriate matrix element of the atomic magnetic moment. Using equations (14) and (15), we can write $\omega(z_j) = 2\Omega_j$ and

$$\varepsilon_{j,n} = \Omega_{j,n}/\nu_n \tag{23}$$

revealing the connection between the coupling constant $\varepsilon_{j,n}$ and the sideband Rabi frequency. Note that the effective Lamb-Dicke parameter $\varepsilon_{j,n}$ is determined by the position dependence of the level splitting $\omega(z_j)$, but not by the detuning δ. The detuning defines the relevant reference frame when applying single-qubit rotations. When choosing a dynamic gradient field (that induces this spin-motion coupling) with zero detuning, then single-qubit rotations resulting from the additional term $(\hbar\delta/2)\Sigma_x$ are avoided. If $\delta \neq 0$, this additional single-qubit rotation will affect the overall evolution. Depending on how exactly a two-qubit gate is carried out, this might lead to a reduced effective coupling due to fast oscillations (for more details see appendix A).

4.1. Spin-motion coupling using time-independent dressed states

Below we discuss another approach helpful to better understand the effect of detuning of the dynamic gradient field. For this purpose we consider time-independent dressed states.

The interaction of a classical driving field with frequency ω_B with a two-level atom with energy splitting $\hbar\omega_0$ in the rotating frame of the driving field is given in the RWA by

$$H = -\frac{\hbar\delta}{2}\sigma_z + \frac{\hbar\Omega}{2}(\sigma_+ + \sigma_-). \tag{24}$$

with $\delta = \omega_B - \omega_0$ and the Rabi frequency Ω. The eigenstates of this Hamiltonian, given by

$$|-\rangle_{\text{dress}} = \cos\theta|g\rangle - \sin\theta|e\rangle, \quad |+\rangle_{\text{dress}} = \sin\theta|g\rangle + \cos\theta|e\rangle \tag{25}$$

with $\tan(2\theta) = \Omega/\delta$, are called dressed states. We transform equation (12) first into the rotating frame of the driving field and consecutively into the dressed-state picture resulting in

$$\begin{aligned} H_{\text{dress}} = {} & \hbar\sqrt{\delta^2 + \Omega^2}\,\tilde{\Sigma}_z + \hbar\nu_n a_n^\dagger a_n \\ & + \frac{\mu_x B' b_{j,n} q_n}{2}(a_n^\dagger + a_n)[\sin(2\theta)\tilde{\Sigma}_z + \cos(2\theta)\tilde{\Sigma}_x] \end{aligned} \tag{26}$$

with $\tilde{\Sigma}_j$ denoting the Pauli-matrices in the dressed state picture. The factor between square brackets in the third term on the right-hand side of equation (26) is of the form $\vec{n}\cdot\vec{\tilde{\Sigma}}$ with $|\vec{n}|^2 = 1$ and can thus be interpreted as a generator of a spin-rotation around the axis $\vec{n} = (\cos(2\theta),\ 0,\ \sin(2\theta))^T$. The motional degree of freedom is now coupled to $\vec{n}\cdot\vec{\tilde{\Sigma}}$. As a consequence, a detuning causes a change in the direction $\vec{n}$ of the coupling, but does not change the coupling strength itself given by the effective Lamb-Dicke parameter $\varepsilon_{j,n}$.

The differences between the states $|\pm\rangle$ defined in equation (17) and $|\pm\rangle_{\text{dress}}$ defined in equation (25) are: (i) $|\pm\rangle$ are defined in the reference frame of the ion and $|\pm\rangle_{\text{dress}}$ in the reference frame of the driving field. (ii) $|\pm\rangle$ are time dependent for $\delta \neq 0$ whereas $|\pm\rangle_{\text{dress}}$ are time independent for $\delta \neq 0$. (iii) A detuning $\delta \neq 0$ leads in the basis $|\pm\rangle$ to an additional driving term $(\delta/2)\sigma_x^{\pm}$, whereas in the dressed-state picture it leads to a change of the rotation axis $\vec{n}$. In both cases, the strength of the coupling determined by the effective Lamb-Dicke parameter $\varepsilon_{j,n}$ is independent of the detuning δ.

4.2. Long-range spin–spin coupling using a dynamic gradient field

In the static case we obtain spin–spin coupling between all pairs of ions, equations (10) and (11), when generalizing the expression for a single ion, equation (3), to the case of N ions. In the case of a dynamic gradient we are lead to the same Hamiltonian as in the static case: equation (20), with the magnitude of the static gradient replaced by the magnitude of the dynamic gradient. Then the generalization to a string of N ions aligned along the z-axis again reveals a spin–spin interaction, as described by equations (10) and (11), induced by the dynamic gradient. The strength of this spin–spin coupling between states dressed by the dynamic gradient field is obtained by simply plugging $\varepsilon_{j,n}$, equation (22), into (11). Since the equations defining the coupling constants $J_{j,k}$ are identical for the static and dynamic case, we do not repeat equation (11) here. This interaction could be used for conditional quantum dynamics without the need for driving sideband resonances as was experimentally demonstrated in the static gradient case [14, 26]. Concrete examples for spin–spin coupling between up to 16 ions exposed to an axial dynamic gradient field are discussed below and in the appendix.

If a dynamic field with a gradient in the *radial* direction is applied to an ion string, then the contributions from different radial vibrational modes to the spin–spin coupling in equation (11) partially cancel each other. This cancellation is particularly significant, if only two ions are present and the trap parameters are such that the center-of-mass (COM) mode and the stretch mode are nearly degenerate.

5. Examples for implementations

The equivalence of static and dynamic MAGIC shown above allows for applying results obtained using static MAGIC, such as [26, 33, 34], to dynamic MAGIC. One consequence is that the scheme proposed here—dynamic MAGIC combined with dressed states—does not require to null the dynamic magnetic field at the ion position. On the contrary, the off-set field B_j at position z_j is useful to create the energy splitting of the dressed state.

5.1. Single- and two-qubit gates

Single-qubit gates using the dressed states $|\pm\rangle$ as a qubit can be carried out by employing a resonant RF-field [35–37]. In order to implement conditional quantum gates, for example 2-qubit gates, the application of an RF-field tuned (close) to resonance with a motional sideband transition between dressed states can be used

[1, 17, 22, 38, 39]. In this case, the effective Lamb-Dicke parameter $\varepsilon_{j,n}$ allows for the necessary coupling between qubit states and motional states [10]. Gates with dressed states in a *static* field gradient have been proposed and successfully implemented with high fidelity [17, 35, 37–39].

As a concrete example for dynamic MAGIC with dressed states we consider $^{171}Yb^{+}$ ions exposed to a resonant driving field with a gradient of $B' = 65\ \mathrm{T\ m^{-1}}$, $\nu_1 = 2\pi \times 500$ kHz leading to $\varepsilon_{j,1} \approx 0.01$ and a Rabi frequency characterizing the RF gate field of $2\pi \times 0.1$ MHz. According to [38] (where dressed states in a static gradient are considered), we expect a gate time of 200 μs and a gate fidelity in the regime of 0.998.

In existing implementations of dynamic MAGIC, a static bias magnetic field having a well defined magnitude is applied to a qubit resonance in order to make it to first order field insensitive and therefore only weakly sensitive to ambient magnetic fields, and thus enhance its coherence time [13, 24, 29, 40]. An additional benefit from using dressed states that exist in a non-zero dynamic gradient field would be that dressed qubits are already resistant against dephasing by ambient noise fields [17, 35–39] without application of an accurately controlled, strong bias field. The dressed state qubit's coherence time would be sensitive to fluctuations in the amplitude of the dressing field. This sensitivity could be strongly reduced by the use of a dressing field at frequency Ω_j [38].

Dynamic MAGIC combined with dressed states can as well be realized with a dynamic gradient along the *axial* direction of an ion string where each ion is exposed to a different dynamic field. Because the axial eigenmodes are characterized by a lower frequency than the radial modes, and the coupling ε between internal and motional states is proportional to $1/\nu^{-3/2}$ (equation (22)), such an arrangement enhances this coupling. Also, the spin–spin coupling J induced by a dynamic gradient is proportional to $1/\nu^{-2}$ (equation (11)), and is therefore stronger in the axial direction than in the radial direction for a given size of the gradient.

In what follows we consider concrete examples for coupling constants that could be achieved experimentally. Using a dynamic gradient $B' = 35\ \mathrm{T\ m^{-1}}$ (as achieved in previous experiments [13]) and an axial trap frequency $\nu_1 = 300$ kHz, the spin-motion coupling for two $^{9}Be^{+}$ ions amounts to $\varepsilon_{j,1} = 0.05$, a magnitude useful for many experiments, for instance, for conditional quantum gates. A dynamic gradient $B' = 200\ \mathrm{T\ m^{-1}}$ appears realistic in future experiments leading again to $\varepsilon_{j,1} \approx 0.05$, now for an axial trap frequency $\nu_1 = 2\pi \times 1$ MHz. More concrete examples of coupling strengths which can be expected from this scheme are given in appendix B.

5.2. Long-range spin–spin coupling

The generalization of Hamiltonian equation (3) to N ions exposed to a static gradient gives rise to spin–spin coupling in a static gradient. Dressed states created by a dynamic gradient exhibit the same type of spin–spin coupling. In section 4, we have shown that a suitable transformation of Hamiltonian equation (20) reveals such a long range spin–spin coupling between all pairs of ions exposed to a resonant dynamic gradient field exactly as given for the static case in equation (11).

The J coupling constant (proportional to B'^2/ν_1^2 for a static or resonant dynamic field) in the presence of a gradient $B' = 200\ \mathrm{T\ m^{-1}}$ and with $\nu_1 = 2\pi \times 1$ MHz amounts to $2\pi \times 1.5$ kHz allowing for a CNOT gate time of about 171 μs. This in turn gives a ratio between experimentally achieved coherence times of dressed states and gate duration of about 3×10^4. So far, $N = 2$ ions undergoing conditional quantum dynamics in a trapping zone have been considered as a building block of a scalable device [41]. Trapping $N > 2$ ions in a trapping zone and taking advantage of long-range spin–spin coupling opens new possibilities for quantum simulations with individually addressed spins and for multi-qubit gates accelerating quantum algorithms [26]. In the appendix we give exemplary coupling matrices for up to 16 ions.

This long-range spin–spin coupling can be tailored for a specific purpose by adjusting global and local trapping potentials in ion traps, even while carrying out a simulation or computation [33, 42, 43]. Such on-the-fly tailoring of potentials can be achieved by changing small voltages applied to segmented trap electrodes.

5.3. Individual addressing of ions

A non-zero dynamic field can have a further advantage, since it allows for individual qubit rotations using an RF driving field at frequency Ω_j specific for each individual ion. Thus, closely spaced, interacting ions exposed to a dynamic gradient close to resonance could be individually addressed [44] in the same way as it was done with a static field gradient by simply dialing in the appropriate RF frequency for each qubit [12, 14, 20]. Using the parameters given above (two $^{9}Be^{+}$ ions, $B' = 200\ \mathrm{T\ m^{-1}}$, $\nu_1 = 2\pi \times 1$ MHz) we estimate a difference of $\Delta\omega \approx 2\pi \times 10$ MHz in the addressing frequency for a resonant dynamic gradient field. The probability p to excite ion A off-resonantly with a single-qubit rotation aimed on ion B is determined by $p = \Omega^2/(\Omega^2 + \Delta\omega^2) \approx 10^{-4}$ assuming a typical resonant Rabi-frequency $\Omega = 2\pi \times 100$ kHz for ion B. More examples for individual addressing are given in the appendix.

The novel concept introduced here—with the features summarized in the introduction and discussed in more detail above—should allow for a decisive reduction of experimental complexity and, at the same time,

opens new perspectives for an RF-based approach to quantum computation and quantum simulations with trapped ions.

Acknowledgments

We acknowledge financial support from the Deutsche Forschungsgemeinschaft.

Appendix A. Two-qubit gates in the dressed-state picture

In the main text of this article, we concentrate on conditional multi-qubit gates described by H_I equation (10), which is directly induced by a *single* static or resonant dynamic gradient field. However, also Mølmer–Sørensen like gates [22] can be performed with MAGIC [11, 17, 25, 38, 39] with and without dressed states. In this section, we discuss some possibilities of carrying out Mølmer–Sørensen-type gates in the dressed-state picture of dynamic MAGIC. In general, there exist a large family of possibilities to carry out two-qubit gates with MAGIC. Therefore, the examples discussed here represent only a small selection of possible implementations. In the first subsection, we transform the Mølmer–Sørensen gate suggested in [11] into the dressed state picture to investigate similarities and differences between static and dynamic MAGIC. Then, we outline proposals for two new strategies for Mølmer–Sørensen-type gates, where the coupling between motional and internal degrees of freedom is created by a resonant dynamic gradient field and two spatially homogeneous RF fields that drive the actual gate.

A.1. A direct Mølmer–Sørensen gate

In this section, we discuss—using the dressed-state picture—the direct implementation of a Mølmer–Sørensen gate with dynamic MAGIC as proposed in [11] and realized in [13] and described by the Hamiltonian given in equation (12). In this case, two detuned dynamic gradient fields are applied that induce the Mølmer–Sørensen gate.

The Hamiltonian from equation (12) is given in the rotating frame of the ion by

$$H = \hbar\nu_n a_n^\dagger a_n + \hbar\Omega_{j,n}(\sigma_+^{(j)} e^{-i(\omega_B-\omega_0)t} + \sigma_-^{(j)} e^{i(\omega_B-\omega_0)t})(a_n^\dagger + a_n) \tag{A.1}$$

under the assumption $\Omega_j = 0$. We define the dressed-states by $|+\rangle = (|0\rangle + |1\rangle)/\sqrt{2}$ and $|-\rangle = (|0\rangle - |1\rangle)/\sqrt{2}$, which transforms the operators $\sigma_\pm$ into

$$\sigma_+ = \frac{1}{2}(\Sigma_Z + \Sigma_+ - \Sigma_-), \quad \sigma_- = \frac{1}{2}(\Sigma_Z - \Sigma_+ + \Sigma_-). \tag{A.2}$$

As a consequence, the Hamiltonian in the dressed-state picture is given by

$$\begin{aligned} H = \hbar\nu_n a_n^\dagger a_n + \hbar\Omega_{j,n}\{&\Sigma_z^{(j)}\cos[(\omega_B-\omega_0)t] \\ &+ i(\Sigma_-^{(j)} - \Sigma_+^{(j)})\sin[(\omega_B-\omega_0)t]\}(a_n^\dagger + a_n). \end{aligned} \tag{A.3}$$

The application of two fields with frequencies $\omega_B^\pm - \omega_0 = \pm(\nu_n - \delta)$ with arbitrary but fixed motional mode n leads to a cancellation of the term proportional to $\sin[(\omega_B - \omega_0)t]$. The interaction between the motional and internal degrees of freedom is thus given by the effective Lamb-Dicke parameter $\varepsilon = \Omega_{j,n}/\nu_n$ and the oscillation described by $\cos[(\omega_B - \omega_0)t]$. Decoupling of motional and internal degrees of freedom analog to equation (7) is not possible due to the time dependence of the interaction. However, a transformation into the interaction picture of the motional modes leads to a Mølmer–Sørensen type Hamiltonian given for two ions by

$$H = \hbar(\Omega_{1,n}\Sigma_z^{(1)} + \Omega_{2,n}\Sigma_z^{(2)})(a_n^\dagger e^{i\delta t} + a_n e^{-i\delta t}). \tag{A.4}$$

The time evolution under this Hamiltonian with duration $T = 2\pi/\delta$, therefore, yields a controlled-phase gate [22]

$$U_{zz} = \exp\left[i\frac{2\pi}{\delta}\frac{\tilde{J}_{1,2}}{2}\Sigma_z^{(1)}\Sigma_z^{(2)}\right]. \tag{A.5}$$

The interaction strength can be determined analog to [45] with the identification $\Omega\eta = \Omega_{j,n} = \varepsilon_{j,n}\nu_n$, where Ω is the driving strength and η the Lamb-Dicke parameter. Hence, using equation (23), we find

$$\tilde{J}_{1,2} = 2\frac{\Omega_{1,n}\Omega_{2,n}}{\delta} = 2\varepsilon_{1,n}\varepsilon_{2,n}\nu_n\frac{\nu_n}{\delta}. \tag{A.6}$$

The use of two RF-sources leads to a factor of two and the active driving of a motional side band leads to a factor of ν_n/δ. This increases the coupling strength compared to equation (11) since δ can be chosen such that $\delta \ll \nu_n$. However, this conditional phase gate is only independent of the vibrational state, if the time T is chosen correctly,

whereas the spin–spin interaction described by equation (11) is independent of the vibrational states for all times.

A.2. An indirect Mølmer–Sørensen gate

In this section, we discuss a new idea to create a Mølmer–Sørensen gate where the gate itself is performed with two fields without gradient and the coupling between the internal and motional degrees of freedom is created by a resonant dynamic gradient field. This approach is based on methods used in [14, 38, 39]. In these cases, a static gradient field was used to create the coupling between internal and motional degrees of freedom.

To create the coupling, we assume a resonant gradient field with $\omega_B = \omega_0$ (as in equation (12)) leading to the Hamiltonian

$$H_c = \hbar\nu_n a_n^\dagger a_n + \frac{\hbar}{2}\Omega_j \sigma_x^{(j)} + \hbar\Omega_{j,n}\sigma_x^{(j)}(a_n^\dagger + a_n) \tag{A.7}$$

in the rotating frame of the ion. We will discuss two different ways for the additional blue and red detuned pulses to create the gate.

A.2.1. Detuned driving fields in z-direction. In our first approach, the additional detuned gate fields are applied along the z-direction and are described by

$$H_z = \hbar\Omega_z \cos(\omega_z t)\sigma_z^{(j)} \tag{A.8}$$

with frequencies $\omega_z = \Omega_j \pm (\nu_n - \delta)$ and Rabi frequency $\Omega_z = \mu_z B_z/\hbar$. The transformation into the rotating frame of the ion does not change this Hamiltonian. The transformation into the dressed state picture transforms H_c (equation (A.7)) into

$$H_{c,\mathrm{DS}} = \hbar\nu_n a_n^\dagger a_n + \frac{\hbar}{2}\Omega_j \Sigma_Z^{(j)} + \hbar\Omega_{j,n}\Sigma_z^{(j)}(a_n^\dagger + a_n), \tag{A.9}$$

which has exactly the form of equation (3). The transformation of H_z leads to

$$H_{z,\mathrm{DS}} = -\hbar\Omega_z \cos(\omega_z t)\Sigma_x^{(j)}. \tag{A.10}$$

The state dependent shifting of the eigenmodes described by the transformation given in equation (7) transforms $H_{c,\mathrm{DS}}$ into equation (9) and $H_{z,\mathrm{DS}}$ into

$$H_{z,\mathrm{SE}} = -\hbar\Omega_z \cos(\omega_z t)[\Sigma_+^{(j)} e^{\varepsilon_{j,n}(a_n^\dagger - a_n)} + \Sigma_-^{(j)} e^{-\varepsilon_{j,n}(a_n^\dagger - a_n)}]. \tag{A.11}$$

We assume to be in the effective Lamb-Dicke regime and therefore $\exp[\varepsilon_{j,n}(a_n^\dagger - a_n)] \approx 1 + \varepsilon_{j,n}(a_n^\dagger - a_n)$. A transformation into the interaction picture of the dressed-state qubit and the motional modes finally leads in the RWA to

$$H_{z,\mathrm{MS}} = -\hbar\varepsilon_{j,n}\Omega_z(\Sigma_+^{(j)} - \Sigma_-^{(j)})(a_n^\dagger e^{\mathrm{i}\delta t} + a_n e^{-\mathrm{i}\delta t}), \tag{A.12}$$

where we have already taken both driving fields with $\omega_z = \Omega_j \pm (\nu_n - \delta)$ into account. This interaction can create a Mølmer–Sørensen gate with the transition strengths

$$\Omega_{\mathrm{MS}} = \frac{\Omega_z^2 \varepsilon_{1,n}\varepsilon_{2,n}}{\delta}. \tag{A.13}$$

The Mølmer–Sørensen gate is not influenced by the spin–spin interaction described by H_J, equation (10), which is also present, because $[\Sigma_z \otimes \Sigma_z, \Sigma_+ \otimes \Sigma_+ \pm \Sigma_- \otimes \Sigma_-] = 0$. Furthermore, the Mølmer–Sørensen gate is in general much faster and the term H_J could therefore be neglected for short time scales.

A.2.2. Detuned driving fields in x-direction. A second method analog to [38] is to use a driving field in x-direction given by

$$H_x = \hbar\Omega_x \cos(\omega_x t)\sigma_x^{(j)} \tag{A.14}$$

with $\omega_x = \omega_0 + \Omega_j \pm (\nu_n - \delta)$. The transformation into the rotating frame of the ion leads to

$$H_{x,\mathrm{RF}} = \hbar\Omega_x[\sigma_+^{(j)} e^{\mathrm{i}(\omega_0 - \omega_x)t} + \sigma_-^{(j)} e^{-\mathrm{i}(\omega_0 - \omega_x)t}], \tag{A.15}$$

where fast oscillating terms with frequency $\omega_0 + \omega_x$ have been neglected. The transformation into the dressed-state picture leads to

$$H_{x,DS} = \hbar\Omega_x\{\Sigma_z^{(j)}\cos[(\omega_0 - \omega_x)t] + \mathrm{i}[\Sigma_+^{(j)} - \Sigma_-^{(j)}]\sin[(\omega_0 - \omega_x)t]\}. \tag{A.16}$$

Table B1. Coupling constants ε between ions and the COM mode, spin–spin coupling $\tilde{J}_{j,k} = J_{j,k}/(2\pi)$ and frequency difference $\Delta\tilde{\omega} = \Delta\omega/(2\pi)$ with $\Delta\omega = \omega_{z_1} - \omega_{z_2}$ for $N = 2$ ions exposed to a constant gradient of $B' = 35\ \mathrm{T\ m^{-1}}$ or $B' = 200\ \mathrm{T\ m^{-1}}$.

	$B' = 35\ \mathrm{T\ m^{-1}}$			$B' = 200\ \mathrm{T\ m^{-1}}$		
Ion	ε	$\tilde{J}_{1,2}$/Hz	$\Delta\tilde{\omega}$/MHz	ε	$\tilde{J}_{1,2}$/kHz	$\Delta\tilde{\omega}$/MHz
$^{171}Yb^{+}$	0.05	164	2.76	0.26	5.36	15.8
$^{9}Be^{+}$	0.05	498	4.00	0.27	16.3	22.8

The shifting of the eigenmodes described by equation (7) leads to

$$H_{x,SE} = \hbar\Omega_x\{\Sigma_z^{(j)}\cos[(\omega_0 - \omega_x)t] + \mathrm{i}[\Sigma_+^{(j)}\mathrm{e}^{\varepsilon_{j,n}(a_n^\dagger - a_n)} - \Sigma_-^{(j)}\mathrm{e}^{-\varepsilon_{j,n}(a_n^\dagger - a_n)}]\sin[(\omega_0 - \omega_x)t]\}. \tag{A.17}$$

The Σ_z term vanishes in the interaction picture (dressed-state qubit and shifted eigenmodes) due to the RWA and we finally arrive in the Lamb-Dicke regime at

$$H_{x,\mathrm{MS}} = \hbar\varepsilon_{j,n}\Omega_x(\Sigma_+^{(j)} - \Sigma_-^{(j)})(a_n^\dagger\mathrm{e}^{\mathrm{i}\delta t} + a_n\mathrm{e}^{-\mathrm{i}\delta t}), \tag{A.18}$$

where we have already taken both driving fields with $\omega_x = \omega_0 + \Omega_j \pm (\nu_n - \delta)$ into account. This Hamiltonian is up to a minus sign exactly the same as equation (A.12) and implements therefore also a Mølmer–Sørensen gate.

Appendix B. Examples

In this appendix we present exemplary values for the coupling constants ε, equation (4), between trapped ions and the COM mode, which is equal for all ions, as well as the spin–spin coupling J_{jk}, equation (7), and the energy splitting of the dressed qubits $\hbar\omega(z)$, equation (15), for different types of ions, different magnitudes of the dynamic gradient field configurations, and different secular trap frequencies. Furthermore, we show concrete exemplary results for a spatially constant dynamic gradient field and results for a gradient field that is created by a single conductor and thus varies spatially.

We first calculate numerically the equilibrium positions of all ions in a linear trap with harmonic axial confinement. These depend on the ions' mass and on the secular trapping frequency ν_1 (COM mode). Then, we determine the frequencies ν_n of the normal vibrational modes and the expansion coefficients $b_{j,n}$ for $n > 1$, equation (2).

As illustrative examples, we show results for a trapping frequency $\nu = 2\pi \times 120$ kHz using $^{171}Yb^{+}$ ions and for $\nu = 2\pi \times 300$ kHz using $^{9}Be^{+}$ ions. The qubit in $^{171}Yb^{+}$ is represented by $|S_{1/2},\ F = 0\rangle$ and $|S_{1/2},\ F = 1,\ m_f = \pm 1\rangle$. This transition is to first order field sensitive, which is important when using static MAGIC. For $^{9}Be^{+}$ we assume that the qubit is realized by the states $|S_{1/2},\ F = 2,\ m_f = 1\rangle$ and $|S_{1/2},\ F = 1,\ m_f = 1\rangle$ as used e.g. in [29]. A constant magnetic field can be applied to make this transition first-order field insensitive. First-order field insensitive states can be only used for dynamic MAGIC. The magnetic moment $\mu_{z/x}$ is given by the Bohr magneton μ_B for both qubits.

The coupling constants ε and J_{jk} and the difference in dressed-qubit resonance frequencies (relevant for individual addressing) for two ions exposed to the same dynamic gradient are given in table B1. The complete coupling matrix $\{J_{jk}\}$ for $N = 16$ ions is displayed in table B2.

As an example for how a dynamic gradient can be generated, we consider the probably simplest possible arrangement: a single wire oriented perpendicular to a linear string of ions. In that case the gradient B' acting on a particular ion depends on that ion's position. In what follows, B' specifies the gradient at the location of the first ion placed $h = 30\mu$m above and $\Delta z = 10\mu$m (approximately equal to the distance between two ions) aside of the conductor, whereas all other ions are exposed to a smaller gradient falling off as $B' = 1/r^2$ with r being the ion's distance from the conductor. The gradient parallel to the axial motion, given by $\partial_z B = B' \cdot z/r$, contributes to the coupling between internal and motional states. The spin–spin coupling matrix $\{J_{jk}\}$ resulting from this configuration for $^{9}Be^{+}$ and $B' = 200\ \mathrm{T\ m^{-1}}$ is given in table B3.

In this case, the spin–spin coupling strength is reduced by about one order of magnitude between the first and the last two ions due to the decrease of the gradient. For a constant gradient, the spin–spin coupling between different pairs of ions also changes due to the spacing of the ions varying along the ion string. However, the order of magnitude of the coupling stays the same (see table B2). For the case of a gradient generated by a single conductor, the addressing frequencies and coupling strengths ε to the COM mode are given in table B4. For a constant gradient, ε is equal for all ions whereas ε differs from ion to ion when the gradient varies spatially. Due to the specific geometry described in the above example, the spin-motion coupling first increases due to better

Table B2. Spin–spin coupling $J_{jk}/(2\pi)$ in kHz for $^9Be^+$ and a constant gradient of $B' = 200$ T m^{-1} for $N = 16$ ions.

Ion	1	2	3	4	5	6	7	8	9	10	11	12	13	14	15	16
1		5.75	4.4	3.67	3.19	2.84	2.57	2.36	2.18	2.02	1.89	1.77	1.66	1.56	1.46	1.36
2	5.75		4.96	4.05	3.49	3.1	2.8	2.56	2.36	2.19	2.04	1.91	1.79	1.68	1.57	1.46
3	4.4	4.96		4.51	3.82	3.36	3.02	2.75	2.54	2.35	2.19	2.05	1.92	1.8	1.68	1.56
4	3.67	4.05	4.51		4.22	3.66	3.27	2.97	2.72	2.52	2.34	2.19	2.05	1.92	1.79	1.66
5	3.19	3.49	3.82	4.22		4.04	3.55	3.2	2.93	2.7	2.51	2.34	2.19	2.05	1.91	1.77
6	2.84	3.1	3.36	3.66	4.04		3.92	3.49	3.17	2.91	2.7	2.51	2.34	2.19	2.04	1.89
7	2.57	2.8	3.02	3.27	3.55	3.92		3.85	3.45	3.16	2.91	2.7	2.52	2.35	2.19	2.02
8	2.36	2.56	2.75	2.97	3.2	3.49	3.85		3.83	3.45	3.17	2.93	2.72	2.54	2.36	2.18
9	2.18	2.36	2.54	2.72	2.93	3.17	3.45	3.83		3.85	3.49	3.2	2.97	2.75	2.56	2.36
10	2.02	2.19	2.35	2.52	2.7	2.91	3.16	3.45	3.85		3.92	3.55	3.27	3.02	2.8	2.57
11	1.89	2.04	2.19	2.34	2.51	2.7	2.91	3.17	3.49	3.92		4.04	3.66	3.36	3.1	2.84
12	1.77	1.91	2.05	2.19	2.34	2.51	2.7	2.93	3.2	3.55	4.04		4.22	3.82	3.49	3.19
13	1.66	1.79	1.92	2.05	2.19	2.34	2.52	2.72	2.97	3.27	3.66	4.22		4.51	4.05	3.67
14	1.56	1.68	1.8	1.92	2.05	2.19	2.35	2.54	2.75	3.02	3.36	3.82	4.51		4.96	4.4
15	1.46	1.57	1.68	1.79	1.91	2.04	2.19	2.36	2.56	2.8	3.1	3.49	4.05	4.96		5.75
16	1.36	1.46	1.56	1.66	1.77	1.89	2.02	2.18	2.36	2.57	2.84	3.19	3.67	4.4	5.75	

Table B3. Spin–spin coupling $J_{j,k}/(2\pi)$ in kHz for $N = 8$ $^9Be^+$ ions exposed to a dynamic magnetic field gradient generated by a single conductor with $B' = 200$ T m^{-1} at the position of ion 1.

Ion	1	2	3	4	5	6	7	8
1		3.52	2.45	1.70	1.20	0.86	0.61	0.43
2	3.52		3.93	2.67	1.87	1.32	0.94	0.66
3	2.45	3.93		2.92	2.00	1.40	0.99	0.69
4	1.70	2.67	2.92		2.00	1.38	0.97	0.67
5	1.20	1.87	2.00	2.00		1.37	0.94	0.64
6	0.86	1.32	1.40	1.38	1.37		0.96	0.64
7	0.61	0.94	0.99	0.97	0.94	0.96		0.69
8	0.43	0.66	0.69	0.67	0.64	0.64	0.69	

Table B4. Coupling to the COM mode ε and addressing frequencies $\tilde{\omega}(z) = \omega(z)/(2\pi)$ for $N = 8$ $^9Be^+$ ions in a spatially varying dynamic gradient generated by a single conductor with $B' = 200$ T m^{-1} at the position of ion 1.

	Ion	1	2	3	4	5	6	7	8
$B' = 35$ T m^{-1}	$\tilde{\omega}(z)$/MHz	6.97	6.06	5.24	4.56	4.00	3.54	3.14	2.76
	ε	0.025	0.034	0.031	0.027	0.022	0.018	0.014	0.011
$B' = 200$ T m^{-1}	$\tilde{\omega}(z)$/MHz	39.8	34.6	29.9	26.0	22.9	20.2	17.9	15.8
	ε	0.143	0.19	0.18	0.15	0.12	0.10	0.082	0.065

alignment of the directions of the gradient and the motional excitation, before it decreases due to the decreasing gradient.

The above configuration using a single straight wire for generating a dynamic gradient serves as an illustrative example. A future experimental realization of the dynamic gradient scheme using dressed states is likely to use a different configuration of gradient-generating elements.

References

[1] Cirac J I and Zoller P 1995 *Phys. Rev. Lett.* **74** 4091
[2] Blatt R and Wineland D 2008 *Nature* **453** 1008
[3] Wineland D J 2013 Nobel lecture: superposition, entanglement, and raising Schrödingers' cat *Rev. Mod. Phys.* **85** 1103–14
[4] Ladd T D, Jelezko F, Laflamme R, Nakamura Y, Monroe C and O'Brian J L 2010 *Nature* **464** 45
[5] Stenholm S 1986 *Rev. Mod. Phys.* **58** 699
[6] Hanneke D, Home J P, Jost J D, Amini J M, Leibfried D and Wineland D J 2010 *Nat. Phys.* **6** 13
[7] Monz T, Nigg D, Martinez E A, Brandl F M, Schindler P, Rines R, Wang S X, Chuang I L and Blatt R 2016 *Science* **351** 1068
[8] Schneider C, Porras D and Schaetz T 2012 *Rep. Prog. Phys.* **75** 024401
[9] Islam R, Senko C, Campbell W C, Korenblit S, Smith J, Lee A, Edwards E E, Wang C-C J, Freericks J K and Monroe C 2013 *Science* **340** 583

[10] Mintert F and Wunderlich C 2001 *Phys. Rev. Lett.* **87** 257904
Mintert F and Wunderlich C 2003 *Phys. Rev. Lett.* **91** 029902 (erratum)
[11] Ospelkaus C, Langer C E, Amini J-M, Brown K R, Leibfried D and Wineland D J 2008 *Phys. Rev. Lett.* **101** 090502
[12] Johanning M, Braun A, Timoney N, Elman V, Neuhauser W and Wunderlich C 2009 *Phys. Rev. Lett.* **102** 073004
[13] Ospelkaus C, Warring U, Colombe Y, Brown K R, Amini J M, Leibfried D and Wineland D J 2011 *Nature* **476** 181
[14] Khromova A, Piltz C, Scharfenberger B, Gloger T F, Johanning M, Varón A F and Wunderlich C 2012 *Phys. Rev. Lett.* **108** 220502
[15] Belmechri N, Förster L, Alt W, Widera A, Meschede D and Alberti A 2013 *J. Phys. B: At. Mol. Opt. Phys.* **46** 104006
[16] Lake K, Weidt S, Randall J, Standing E, Webster S C and Hensinger W K 2015 *Phys. Rev.* A **91** 012319
[17] Weidt S, Randall J, Webster S C, Lake K, Webb A E, Cohen I, Navickas T, Lekitsch B, Retzker A and Hensinger W K 2016 *Phys. Rev. Lett.* **117** 220501
[18] Schrader D, Dotsenko I, Khudaverdyan M, Miroshnychenko Y, Rauschenbeutel A and Meschede D 2004 *Phys. Rev. Lett.* **93** 150501
[19] Warring U, Ospelkaus C, Colombe Y, Jördens R, Leibfried D and Wineland D J 2013 *Phys. Rev. Lett.* **110** 173002
[20] Piltz C, Sriarunothai T, Varón A F and Wunderlich C 2014 *Nat. Commun.* **5** 679
[21] Aude Craik D P L, Linke N M, Sepiol M A, Harty T P, Ballance C J, Stacey D N, Steane A M, Lucas D M and Allcock D T C 2016 arXiv:1601.02696
[22] Sørensen A and Mølmer K 2000 *Phys. Rev.* A **62** 022311
[23] Brown K R, Wilson A C, Colombe Y, Ospelkaus C, Meier A M, Knill E, Leibfried D and Wineland D J 2011 *Phys. Rev.* A **84** 030303(R)
[24] Harty T P, Allcock D T C, Ballance C J, Guidoni L, Janacek H A, Linke N M, Stacey D N and Lucas D M 2014 *Phys. Rev. Lett.* **113** 220501
[25] Harty T P, Sepiol M A, Allcock D T C, Ballance C J, Tarlton J E and Lucas D M 2016 *Phys. Rev. Lett.* **117** 140501
[26] Piltz C, Sriarunothai T, Ivanov S, Wölk S and Wunderlich C 2016 *Sci. Adv.* **2** 1600093
[27] Johanning A, Varon M and C Wunderlich 2009 *J. Phys. B: At. Mol. Opt. Phys.* **42** 154009
[28] Warring U, Ospelkaus C, Colombe Y, Brown K R, Amini J M, Carsjens M, Leibfried D and Wineland D J 2013 *Phys. Rev.* A **87** 013437
[29] Carsjens M, Kohnen M, Dubielzig T and Ospelkaus C 2014 *Appl. Phys.* B **114** 243
[30] Segal D M and Wunderlich C 2014 Cooling techniques for trapped ions *Physics with Trapped Charged Particles* ed M Knoop *et al* (London: Imperial College Press) (https://doi.org/10.1142/9781783264063_0003)
[31] Wunderlich C 2002 Conditional spin resonance with trapped ions *Laser Physics at the Limit* (Heidelberg-Berlin-New York: Springer-Verlag) p 261
[32] Wunderlich C and Balzer C 2003 *Adv. At. Mol. Opt. Phys.* **49** 295–376
[33] Zippilli S, Johanning M, Giampaolo S M, Wunderlich C and Illuminati F 2014 *Phys. Rev.* A **89** 042308
[34] Yang D, Giri G, Johanning M, Wunderlich C, Zoller P and Hauke P 2016 *Phys. Rev.* A **94** 052321
[35] Timoney N, Baumgart I, Johanning M, Varón A F, Plenio M B, Retzker A and Wunderlich C 2011 *Nature* **476** 185
[36] Webster S C, Weidt S, Lake K, McLoughlin J J and Hensinger W K 2013 *Phys. Rev. Lett.* **111** 140501
[37] Randall J, Weidt S, Standing E D, Lake K, Webster S C, Murgia D F, Navickas T, Roth K and Hensinger W K 2015 *Phys. Rev.* A **91** 012319
[38] Cohen I, Weidt S, Hensinger W K and Retzker A 2015 *New. J. Phys.* **17** 043008
[39] Mikelsons G, Cohen I, Retzker A and Plenio M B 2015 *New. J. Phys.* **17** 053032
[40] Langer C *et al* 2005 *Phys. Rev. Lett.* **95** 060502
[41] Kielpinski D, Monroe C and Wineland D J 2002 *Nature* **417** 709–11
[42] Mc Hugh D and Twamley J 2005 *Phys. Rev.* A **71** 012315
[43] Wunderlich H, Wunderlich C, Singer K and Schmidt-Kaler F 2009 *Phys. Rev.* A **79** 052324
[44] Navon N, Kotler S, Akerman N, Glickman Y, Almog I and Ozeri R 2013 *Phys. Rev. Lett.* **111** 073001
[45] Sørensen A and Mølmer K 1999 *Phys. Rev. Lett.* **82** 1997